Coupling heat transfer solvers and large eddy simulations for combustion applications

By F. Duchaine†, S. Mendez†, F. Nicoud‡, A. Corpron¶, V. Moureau¶ AND T. Poinsot†‖

A fully parallel environment for conjugate heat transfer has been developed and applied to two configurations of interest for the design of combustion devices. The numerical tool is based on a reactive LES (Large Eddy Simulations) code and a solid conduction solver that can exchange data via a supervisor. Two coupled problems, typical of gas turbine applications, are studied: (1) a flame/wall interaction problem is used to assess the precision of the coupled solutions depending on the coupling frequency. For such an unsteady case, it is shown that the temperature and the flux across the wall are well-reproduced when the codes are coupled on a time scale which is of the order of the smallest time scale. (2) An experimental film-cooled turbine vane is studied in order to reach a steady state. The solutions from the conjugate analyses and an adiabatic wall convection are compared to experimental results. Pressure profiles on pressure and suction sides obtained by adiabatic and coupled simulations show a good agreement with experimental results. Compared to the adiabatic simulation, it is found that the conjugate heat transfer case has a lower mean pressure side temperature due to the thermal conduction from this part to the plenum as well as from the pressure to the suction side of the blade. Thermal results show a very large sensitivity to multiple parameters as the coupling strategy and LES models.

1. Introduction

Conjugate heat transfer is a key issue in combustion (Lefebvre 1999; Bunker 2007): the interaction of hot gases and reacting flows with colder walls is a key phenomenon in all chambers and is actually a main design constraint in gas turbines. For example, multi-perforated plates are commonly used in gas turbine combustion chambers to cool walls and they must be able to sustain the high fluxes produced in the chamber. After combustion, the interaction of the hot burnt gases with the high pressure stator and the first turbine blades conditions the temperature and pressure levels reached in the combustor, and therefore the engine efficiency.

Conjugate heat transfer is a difficult to accomplish and most existing tools are developed for chained (rather than coupled), steady (rather than transient) phenomena: the fluid flow is brought to convergence using a RANS (Reynolds Averaged Navier-Stokes) solver for a given set of skin temperatures (Schiele & Wittig 2000; Garg 2002; Mercier *et al.* 2006). The heat fluxes predicted by the RANS solver are then transferred to a heat transfer solver which produces a new set of skin temperatures. A few iterations are generally sufficient to reach convergence. There are circumstances, however, where this chaining method must be replaced by a full coupling approach. Flames interacting with walls for example, may require a simultaneous resolution of the temperature within the solid and around it. More generally, the introduction of LES to replace RANS leads to full coupling since LES provides the unsteady evolution of all flow variables.

Fully coupled conjugate heat transfer requires that multiple questions be taken into account. Among them, two issues were considered for the present work:

• The time scales of the flow and of the solid are generally very different. In a gas turbine, a blade submitted to the flow exiting from a combustion chamber has a thermal characteristic time scale of the order of a few seconds, while the flow-through time along the blade is less than 1 ms.

† CERFACS, CFD Team, 42 Av Coriolis, 31057 Toulouse, France
‡ Un. Montpellier II, France
¶ TURBOMECA, Bordes, France
‖ IMF Toulouse, INP de Toulouse and CNRS, 31400 Toulouse, France

As a consequence, the frequency of the exchanges between the codes is critical for the precision, stability and restitution time of the computations.

• Coupling the two phenomena must be performed on massively parallel machines where the codes must be not only coupled but synchronized to exploit the power of the machines.

During this work, these two issues have been studied using two examples of conjugate heat transfer: (I) a flame interacting with a wall and (II) a blade submitted to a flow of hot gases. Both problems have considerable impact on the design of combustion devices.

2. Solvers and coupling strategies

The AVBP code is used for the fluid (Schönfeld & Rudgyard 1999; Roux *et al.* 2008). It solves the compressible reacting Navier-Stokes equations with a third-order scheme for spatial differencing and a Runge-Kutta time advancement (Colin & Rudgyard 2000; Moureau *et al.* 2005). Boundary conditions are handled with the NSCBC formulation (Poinsot & Veynante 2005; Moureau *et al.* 2005).

For the resolution of the heat transfer equation within solids, a simplified version of AVBP, called AVTP, was developed. It uses the same data structure as AVBP. It is coupled to AVBP using a software called PALM (Buis *et al.* 2005). For all present examples, the skin meshes are the same for the fluid and the solid so that no interpolation error is introduced at this level.

The coupling strategy between AVBP and AVTP depends on the objectives of the simulation and is characterized by two issues:

• Synchronization in physical time: The physical time computed by the two codes between two information exchanges may be the same or not.† We will impose that between two coupling events, the flow is advanced in time of a quantity $\alpha_f \tau_f$ where τ_f is a flow characteristic time. Simultaneously, the solid is advanced of a time $\alpha_s \tau_s$ where τ_s is a characteristic time for heat propagation through the solid. Two limit cases are of interest: (1) $\alpha_s = \alpha_f$ ensures that both solid and fluid converge to steady state at the same rate (the two domains are then not synchronized in physical time) and (2) $\alpha_f \tau_f = \alpha_s \tau_s$ ensures that the two solvers are synchronized in physical time.

• Synchronization in CPU time: on a parallel machine, codes for the fluid and for the structure may be run together or sequentially. An interesting question controlled by the execution mode is the information exchange. Figure 1 shows how heat fluxes and temperature are exchanged in a mode called SCS (Sequential Coupling Strategy) where the fluid solver after run n (physical duration $\alpha_f \tau_f$) provides fluxes to the solid solver which then starts and gives temperatures T_n (physical duration $\alpha_s \tau_s$). In SCS mode, the codes are loaded into the parallel machine sequentially and each solver uses all available processors (N). Another solution is Parallel Coupling Strategy (PCS) where both solvers run together using information obtained from the other solver at the previous coupling iteration (Fig. 1). In this case, the two solvers must share the $P = P_s + P_f$ processors. The P_s and P_f processors dedicated to the solid and the fluid, respectively, must be such that:

$$\frac{P_f}{P} = \frac{1}{1 + T_s/T_f} \tag{2.1}$$

where T_s and T_f are the execution times of the solid and fluid solvers, respectively (on one processor). T_s and T_f depend on $\alpha_s \tau_s$ and $\alpha_f \tau_f$. Perfect scaling for both solvers is assumed here.

Note that both SCS and PCS questions are linked to the way information (heat fluxes and wall temperatures) are exchanged and to the implementation on parallel machines but are independent of the synchronization in physical time: PCS or SCS can be used for steady or unsteady computations. This paper focuses on the PCS strategy.

Finally,this work explores the simplest coupling method where the fluid solver provides heat fluxes to the solid solver while the solid solver sends skin temperatures back to the fluid code.

† For example, when a steady state solution is sought (i.e., to be used as initial condition for an unsteady computation), physical times for both solvers can differ.

Sequential coupling strategy SCS | Parallel coupling strategy PCS

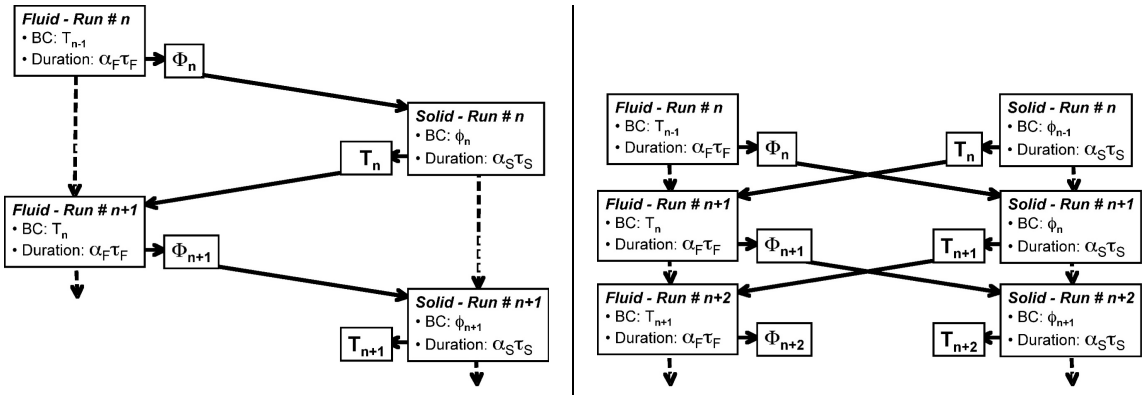

FIGURE 1. Main types of coupling strategies.

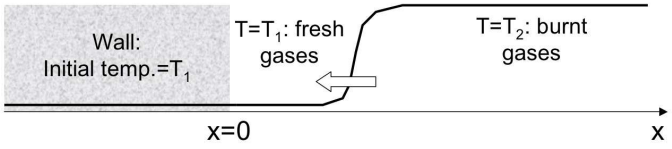

FIGURE 2. Interaction between wall and premixed flame. Solid line: initial temperature profile.

More sophisticated methods may be used for precision and stability (Giles 1997; Chemin 2006) but the present one was found sufficient for the two test cases described below.

3. Flame/wall interaction (FWI)

The interaction between flames and walls controls combustion, pollution and wall heat fluxes in a significant manner (Poinsot & Veynante 2005; Delataillade *et al.* 2002; Dabireau *et al.* 2003). It also determines the wall temperature and its lifetime. In most combustion devices, burnt gases reach temperatures between 1500 and 2500 K while wall temperatures remain between 400 and 850 K because of cooling. The temperature decrease from burnt gases levels to wall levels occurs in a near-wall layer which is less than 1 mm thick, creating large temperature gradients.

Studying the interaction between flames and walls is difficult from an experimental point of view because all interesting phenomena occur in a thin zone near the wall: In most cases, the only measurable quantity is the unsteady heat flux through the wall. Moreover, flames approaching walls are dominated by transient effects; they usually do not "touch" walls and quench a few micrometers away from the cold wall because the low wall temperature inhibits chemical reactions. At the same time, the large near-wall temperature gradients lead to very high wall heat fluxes. These fluxes are maintained for short durations and their characterization is also a difficult task in experiments (Lu *et al.* 1990; Ezekoye *et al.* 1992).

The present study focuses on the interaction between a laminar flame and a wall (Fig. 2). Except for a few studies using integral methods within the solid (Desoutter *et al.* 2005) or catalytic walls (Popp *et al.* 1996; Popp & Baum 1997), most studies dedicated to FWI were performed assuming an inert wall at constant wall temperature. Here we will revisit the assumption of isothermicity of the wall during the interaction.

3.1. *The infinitely fast flame (IFF) limit*

Flame front thicknesses (δ_L^o) are less than 1 mm and laminar flame speeds (s_L^o) are of the order of 1 m/s. Walls are usually made of metal or ceramics and their characteristic time scale $\tau_s = L^2/D_s$ (where L is the wall thickness and D_s the wall diffusivity) is much longer than the flame characteristic time $\tau = \delta_L^o/s_L^o$. An interesting simplification of this observation is the "Infinitely

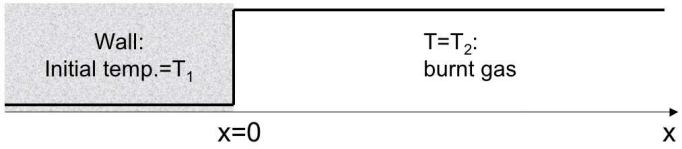

FIGURE 3. The IFF (Infinitely Fast Flame) limit. Solid line: initial temperature profile.

	Initial temperature	Thermal diffusivity	Thermal effusivity	Thermal conductivity	Heat capacity	Density	Mesh size	Fourier time step
Solid	650	$3.38\ 10^{-6}$	7058.17	12.97	460	8350	$4\ 10^{-6}$	$2.37\ 10^{-6}$
Fluid	660	$2.53\ 10^{-5}$	5.52	0.028	1162.2	0.947	$4\ 10^{-6}$	$3.16\ 10^{-7}$

TABLE 1. Fluid and solid characteristics for IFF test case (SI units). The Fourier time step corresponds to the stability limit for explicit schemes $\Delta t^D = \Delta x^2/(2D_{th})$.

Fast Flame" limit (IFF) in which the time scale of the flame is assumed to be zero compared to the solid time. In this case, the FWI limit can be replaced by the simpler case of a semi-infinite solid at temperature T_1 getting instantaneously in touch with a semi-infinite fluid at a constant temperature T_2 where T_2 is the adiabatic flame temperature (Fig. 3). The propagation time of the flame toward the wall is neglected.

The IFF problem is a classical heat transfer problem and has an analytical solution which can be written as:

$$T(x,t) = T_1 + b\frac{T_2 - T_1}{b + b_s} erfc(-\frac{x}{2\sqrt{D_s t}}) \quad \text{for} \quad x < 0 \tag{3.1}$$

$$T(x,t) = T_2 - b_s\frac{T_2 - T_1}{b + b_s} erfc(\frac{x}{2\sqrt{Dt}}) \quad \text{for} \quad x > 0 \tag{3.2}$$

where $b = \sqrt{\lambda\rho C_p}$ is the effusivity of the burnt gases, $b_s = \sqrt{\lambda_s\rho_s C_{ps}}$ the effusivity of the wall and D the burnt gases' diffusivity. D_s and D are assumed to be constant in the solid and fluid parts. The temperature of the wall at $x = 0$ is constant and the heat flux Φ decreases like $1/\sqrt{t}$:

$$T(x=0,t) = \frac{bT_2 + b_s T_1}{b + b_s} \quad \text{and} \quad \Phi(x=0,t) = \frac{T_2 - T_1}{b + b_s}\frac{bb_s}{\sqrt{\pi t}} \tag{3.3}$$

This IFF limit is useful to understand FWI limits. It was also used as a test case of the coupled codes to check the accuracy of coupling strategies (next section).

3.2. *The IFF limit as a test case for unsteady fluid / heat transfer coupling*

A central question for SCS or PCS methods is the coupling frequency between the two solvers especially when they have very different characteristic times. Since the IFF has an analytical solution, it was first used as a test case for PCS methods. The test case corresponds to a wall at 650 K in contact at $t = 0$ with a fluid at 660 K. Compared to a wall/flame interaction, this small temperature difference is chosen in order to keep constant values for D, λ and Cp. Table 1 summarizes the properties of the solid and the fluid and indicates mesh size Δx and maximum time steps Δt^D for diffusion (the only important ones here since the flow does not move).

The most interesting part of this problem is the initial phase when fluxes are large and coupling difficult. During this phase, the solid and the fluid can be considered as infinite and there is no proper length or time scale to evaluate τ_f or τ_s in Fig. 1. The only useful scale is the grid mesh and the associated time scale for explicit algorithm stability. Therefore we chose to take $\tau_f = \Delta t_f^D$ and $\tau_s = \Delta t_s^D$. (Note that the fluid solver is limited by an acoustic time step smaller than Δt_f^D). The strategy used for this test is the PCS method (Fig. 1) for unsteady cases which requires $\alpha_f\tau_f = \alpha_s\tau_s$. The α_f parameter defines the time interval between two coupling events

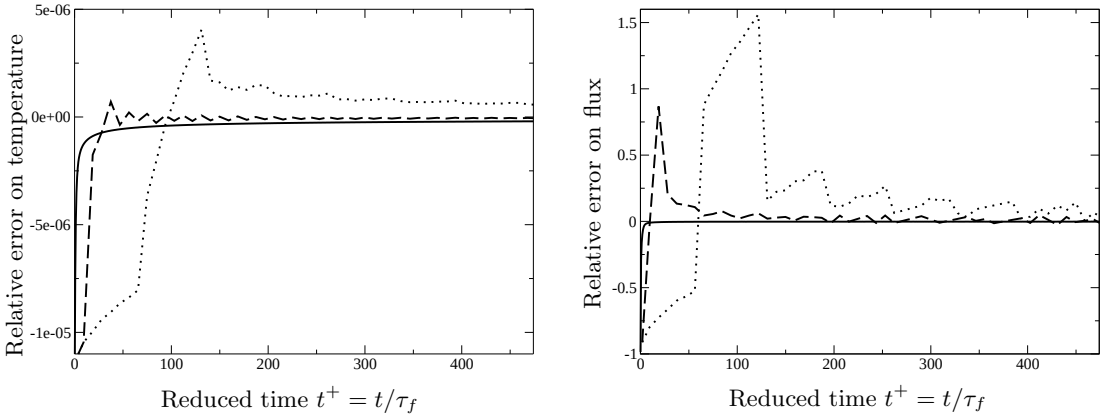

FIGURE 4. Tests of the PCS method for the IFF case of Fig. 3. Effects of the coupling period between two events (measured by α_s). Left: relative error on wall temperature at $x = 0$, right: relative error on wall flux at $x = 0$. Solid line: $\alpha_f = 0.131$, dashed: $\alpha_f = 13.1$, dots: $\alpha_f = 65.5$.

	Initial temperature	Thermal diffusivity	Thermal effusivity	Thermal conductivity	Heat capacity	Density	Mesh size	Time scale
Solid	650	$3.38\ 10^{-6}$	7058.17	12.97	460	8350	$2\ 10^{-6}$	0.3
Fresh gases	650	$4.14\ 10^{-5}$	7.35	0.047	1168.9	0.977	$4\ 10^{-6}$	$30.45\ 10^{-6}$
Hot gases	2300	$3.72\ 10^{-4}$	7.28	0.140	1441.6	0.262	$4\ 10^{-6}$	$30.45\ 10^{-6}$

TABLE 2. Fluid and solid characteristics for flame/wall interaction test case (SI units). The characteristic time τ_s for the solid is based on its thickness and heat diffusivity. The characteristic time scale for the fluid τ_f is based on the flame speed and thickness.

normalized by the fluid characteristic time. Values of α_f ranging from 0.131 to 65.5 were tested for this problem and Fig. 4 shows how the errors on maximum wall temperature and the wall heat flux change when α_f changes. The IFF solution of Eq. (3.3) is used as the reference solution. Using values of α_f larger than unity leads to relative errors which can be significant and to strong oscillations on the temperature and flux. As expected a full coupling of fluid and solid for this problem requires that values of α_f of order unity be used which means to couple the codes on a time scale that is of the order of the smallest time scale (here the flow time scale).

3.3. *Flame/wall interaction results*

This section presents results obtained for a fully coupled FWI and compares them to the IFF limit. The parameters used for the simulation (Table 2) correspond to a methane/air flame at an equivalence ratio of 0.8, propagating in fresh gases at a temperature T_1 of 650 K at a laminar speed $s_L^o = 1.128$ m/s. The adiabatic flame temperature is $T_2 = 2300$ K. The wall is also initially at $T_1 = 650$ K. The maximum time step corresponds to the Fourier stability criterion for the solid and to the CFL stability criterion for the fluid. These time steps are respectively $\Delta t_s^F = 0.59\ \mu s$ and $\Delta t_f^{CFL} = 0.0023\ \mu s$. For this fully coupled problem, the only free parameter is α_f. The period between two coupling events ($\alpha_f \tau_f = \alpha_s \tau_s$) determines the number of iterations performed by the gas solver during this time: $N_{it} = \alpha_f \tau_f / \Delta t_f^{CFL}$. As the cost of computing heat transfer in the solid for this problem is actually negligible, no attempt was made to optimize the computation. The effect of mesh resolution in the gases was also checked and found to be negligible; for most runs, 500 mesh points are used in the gases with a mesh size of $4\ 10^{-6}$ mm.

The coupling parameters for the presented case correspond to a PCS simulation with $\alpha_f = 7.5\ 10^{-3}$ leading to $N_{it} = 100$ in the gases accompanied by one iteration in the solid where $\alpha_s = 7.6\ 10^{-7}$ (Fig. 5). Figure 6 displays the wall-scaled temperature at the fluid and solid interface

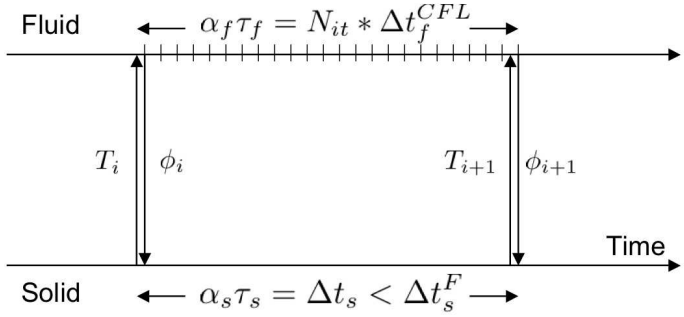

FIGURE 5. Parallel coupling strategy for the flame/wall interaction with $\alpha_f = 7.5\ 10^{-3}$.

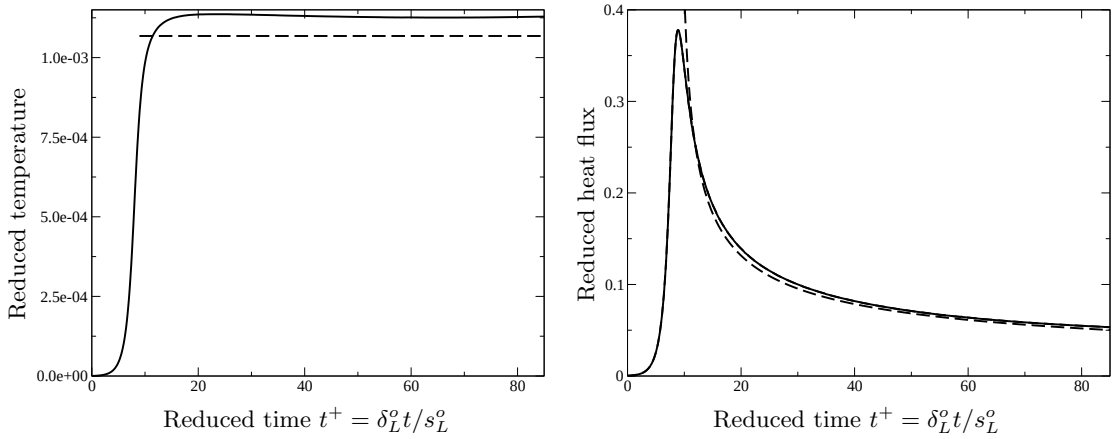

FIGURE 6. Coupled flame/wall interaction simulation (solid line). Comparison with IFF limit adjusted to start at flame quenching (dashed line). Left: reduced wall temperature ($x = 0$), right: reduced wall heat flux at $x = 0$.

$T^* = (T(x=0) - T_1)/(T_2 - T_1)$ and the reduced maximum heat flux $\Phi/(\rho C_p s_L^o (T_2 - T_1)$ through the wall versus time. The flame quenches at time $s_L^o t/\delta_L^o = 9$, where the flux is maximum. Figure 6 also displays the prediction of the IFF limit (Eq. (3.3)). Except in the first instants of the interaction, when the flame is still active, the IFF limit matches the simulation results extremely well, both in terms of fluxes and wall temperature. The IFF solution cannot predict the maximum heat flux because it leads to an infinite flux at the initial time. However, as soon as the flame is quenched, it gives a very good evaluation of the wall heat flux. Note that the wall temperature increases by a small amount during this interaction between an isolated flame and the wall ($T^* \approx 10^{-3}$ on Fig. 6). In more realistic cases, flame will flop and hit walls frequently, which could lead to cumulative effects and therefore to higher wall temperature and fatigue.

Figure 7 shows how the wall temperature at $x = 0$ changes when the effusivity of the solid varies. For the IFF limit, this temperature is given by Eq. (3.3) and for the simulation, it is the temperature reached asymptotically for long times. The agreement is excellent and confirms that the IFF limit correctly predicts the long-term evolution in this FWI problem. It also shows that the coupled simulation works correctly. Note, however, that the IFF limit given by Eq. (3.3) is only approximate for the FWI problem since it assumes constant density and heat diffusivity in the gases.

Finally, Fig. 8 shows how the coupling frequency (measured by the parameter α_f) changes the precision of the coupled simulation (coupling events are scheduled at every $\alpha_f \tau_f$ times where τ_f is the fluid time). The precision of the coupling was checked by changing N from 100 to 500,000 (α_f from $7.5\ 10^{-3}$ to 37.8) with $N_{it} = 10$ ($\alpha_f = 7.5\ 10^{-4}$) as reference. The error on the maximum temperature remains very small, even for large α_f values. The error on the maximum energy entering the wall between the initial time and an arbitrary instant (here $\delta_L^o t/s_L^o = 82$) depends

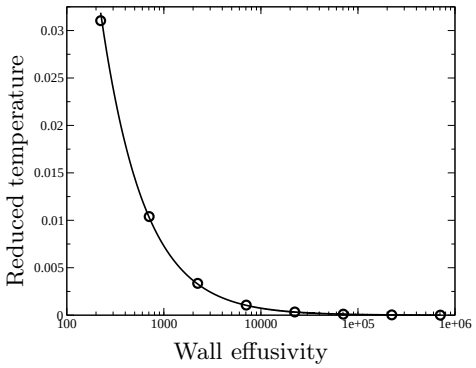

FIGURE 7. Coupled flame/wall interaction simulation. Reduced wall temperature $(T(x=0)-T_1)/(T_2-T_1)$ vs. wall effusivity b_s. Solid line: IFF limit, circles: coupled simulation.

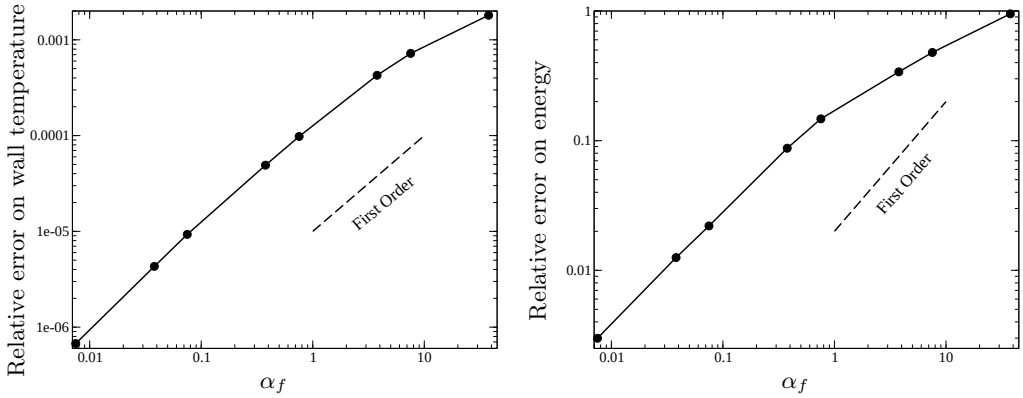

FIGURE 8. Flame/wall interaction simulation. Left: relative error on wall temperature ($x=0$) from $t^+=\delta_L^o t/s_L^o=0$ to $t^+=82$, right: relative error on the energy fluxed into the wall during the same period.

strongly on α_f. As expected from results obtained for the IFF problem only (previous section), coupling the two solvers less often that τ_f ($\alpha_f>1$) leads to errors larger than 10% on the energy fluxed into the wall. The errors on temperature and energy fluxed into the wall converge both to 0 when α_f decreases with an order close to 1.

4. Blade cooling

The second example studied during this work is the interaction between a high-speed flow and a cooled blade. This example is typical of one of the main problems encountered during the design of combustion chambers (Bunker 2007; Bogard & Thole 2006): The hot flow leaving the combustor must not burn the turbine blades or the vanes of the high-pressure stator. Predicting the vanes' temperature field (which are cooled from the inside by cold air) is a major research area (Holmer *et al.* 2000; Medic & Durbin 2002; Garg 2002). Here an experimental setup (T120D blade) developed within the AITEB-1 European project was used to evaluate the precision of the coupled simulations (Fig. 9). The temperature difference between the mainstream ($T_2=333.15\ K$) and cooling ($T_1=303.15\ K$) airs is limited to 30 K to facilitate measurements. Experimental results include pressure data on the blade suction and pressure sides as well as temperature measurement on the pressure side.

The computational domains for both the fluid and the structure contain only one spanwise pitch of the film cooling hole pattern (z-axis on Fig. 9), with periodicity enforced at each end. This simplification assumes no end-wall effects, but retains the three-dimensionality of the flow and greatly reduces the number of tetrahedral cells required to model the blade: about 6.5 million

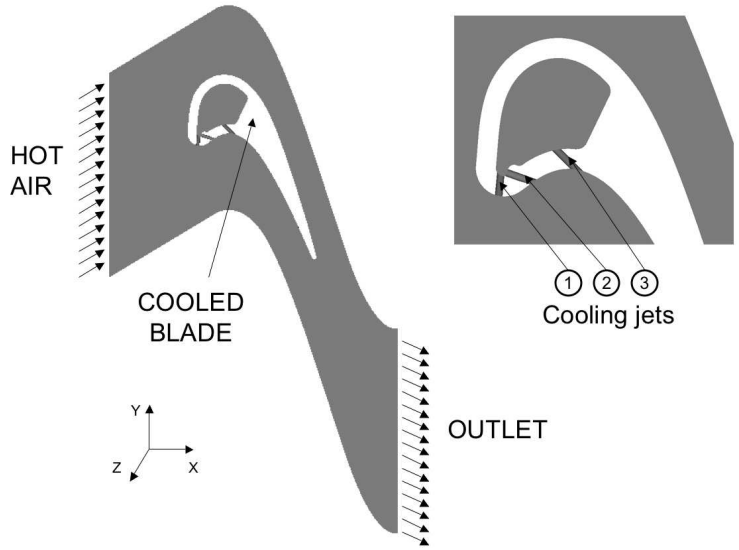

FIGURE 9. Configuration for blade cooling simulation: the T120D blade (AITEB-2 project).

	Inlet static temperature	Inlet total temperature	Inlet total pressure	Flow rate	Thermal conductivity	Heat capacity	Time scale	Time step Δt_f^m
Mainstream	$T_2 = 333.15$	$T_2^t = 339.15$	$P_2^t = 27773$	0.0185	$2.6\ 10^{-2}$	1015	0.001	$9.80\ 10^{-8}$
Cooling air	$T_1 = 303.15$	$T_1^t = 303.15$	$P_1^t = 29143$	0.000148	$2.44\ 10^{-2}$	1015	0.0006	$9.80\ 10^{-8}$

TABLE 3. Flow characteristics for the blade cooling case (SI units). The fluid time scales are based on the flow-through times in and around the blade. The characteristic fluid time scale τ_f is the maximum of this time, i.e., $\tau_f = 0.001$. The time step Δt_f^m is limited by the acoustic CFL number (0.7).

cells to discretize the fluid and 600,000 for the solid. A periodicity condition is also assumed in the y-direction. The WALE subgrid model (Nicoud & Poinsot 1999) is used in conjunction with non-slipping wall conditions. As shown in Fig. 9, the three film-cooling holes and the plenum are included in the domain: jet 2 is aligned with the main flow (in the xy-plane) while jets 1 and 3 have a compound orientation. The mean blowing ratio (ratio of a jet momentum on the hot flow momentum) of the jets based on a hot gases velocity of 35 ms^{-1} is approximately 0.4.

Tables 3 and 4 summarize the properties of the gases and of the solid used for the simulation. At each coupling event, fluxes and temperature on the blade skin are exchanged as described in Fig. 1. During this work, only a steady state solution within the solid was sought so that time consistency was not ensured during the coupling computation. The converged state is obtained with a two-step methodology:

(a) Initialization of the coupled calculation that includes:
- a thermal converged adiabatic fluid simulation,
- a thermal converged isothermal solid computation with boundary temperatures given by the fluid solution,

(b) Coupled simulation.

Convergence is investigated by plotting the history of the total flux on the blade (which must go to zero) and of the mean, minimum and maximum blade temperatures. Figures 10 and 11 show these results for two variants of the PCS strategy. In the first one, fluxes and temperature are exchanged at each coupling step while for the second one, relaxation is used and temperature and fluxes imposed at each coupling iteration n are written as $f^n = af^{n-1} + (1-a)f^{n*}$ where f^{n*} is

Thermal conductivity	Heat capacity	Density	Thermal diffusivity	Time scale τ_s	Time step
0.184	1450	1190	$1.07\ 10^{-7}$	34.22	$1.71\ 10^{-3}$

TABLE 4. Solid characteristics for the blade-cooling case (SI units). The time scale τ_s is computed using the thermal diffusivity and the blade minimum thickness.

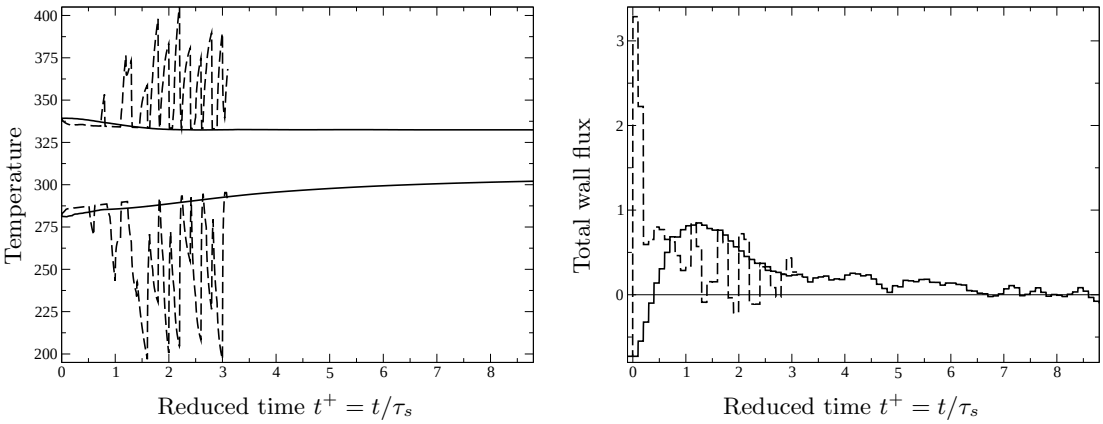

FIGURE 10. Time evolution of minimum and maximum temperatures in the blade (left) and total heat flux through the blade with (solid) and without (dashed) relaxation.

the value obtained by the other solver at iteration n and a is a relaxation factor (typically $a = 0.6$). Without relaxation, the system becomes unstable and convergence almost impossible.

At the converged state, the total flux reaches zero: the flux entering the blade is evacuated into the cooling air in the plenum and in the holes (Fig. 11). Note however that the analysis of fluxes on the blade skin shows that, even though the blade is heated by the flow on the pressure side, it is actually cooled on part of the suction side because the flow accelerates and cools down on this side. Due to the acceleration in the jets, heat transfer in the holes and plenum are of the same order. Compared to the external flux, plenum and hole fluxes converge almost linearly. Oscillations in the external flux evolution are linked with the complex flow structure developing around the blade.

At the converged state, results can be compared to the experiment in terms of pressure profiles on the blade (on both sides) and of temperature profiles on the pressure side. Pressure fields are displayed in terms of isentropic Mach numbers M_{is} computed by

$$M_{is} = \sqrt{\frac{2}{\gamma - 1}\left[\left(\frac{P_2^t}{P_w^t}\right)^{\frac{\gamma-1}{\gamma}} - 1\right]} \tag{4.1}$$

where P_2^t and P_w^t are the total pressure of the mainstream and at the wall. Figure 12 displays an average field of isentropic Mach number obtained by LES and by the experiment. The comparison of the adiabatic simulation and the coupled one shows that these profiles are only weakly sensitive to the thermal condition imposed on the blade. Although the shock position on the suction side is not perfectly captured, the overall agreement between LES and experimental results is fair.

Temperature results are displayed in terms of reduced temperature $\Theta = (T_2^t - T)/(T_2^t - T_1^t)$ where T_2^t and T_1^t are the total temperatures of the main and cooling streams (Table 4) and T is the local wall temperature. Θ measures the cooling efficiency of the blade. Figure 13 shows measurements, adiabatic and coupled LES results for Θ spanwise averaged along axis x. As expected, the cooling efficiency obtained with the adiabatic computation is lower than the experimental values: The

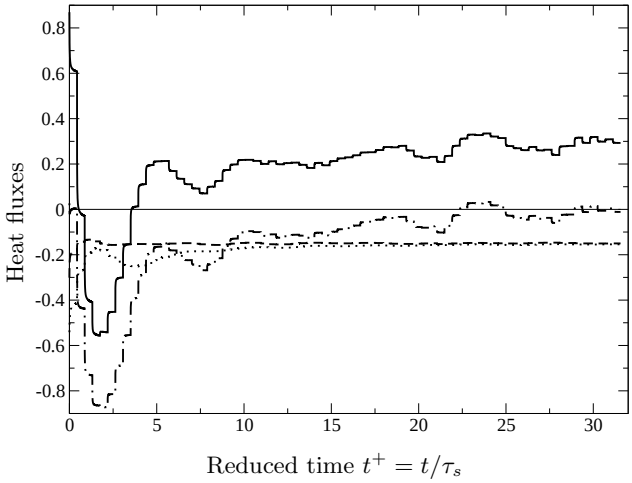

FIGURE 11. Time evolution of heat fluxes through the blade: external flux (solid line), plenum (dashed), holes sides (dot), sum of all fluxes (dot dashed).

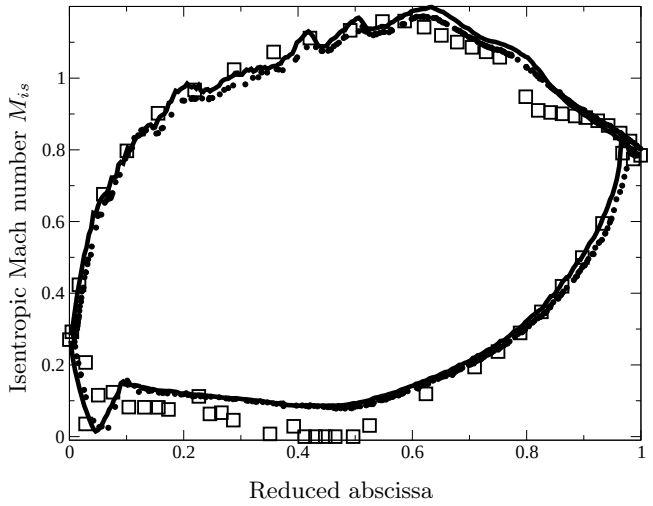

FIGURE 12. Isentropic Mach number along the blade. Solid line: coupled LES, circles: adiabatic LES, squares: experiment.

adiabatic temperature field over-predicts the real one. The main contribution of conduction in the blade is to reduce the wall temperature on the pressure side.

The reduced temperature distribution on the pressure side (Fig. 14) shows that the peak temperature occurs at the stagnation point (reduced abscissa close to 0). The temperature at the stagnation point is reduced compared to the adiabatic wall prediction, leading to local values of θ of the order of 0.2. The thermal effects of the cooling jets on the vane are clearly evidenced by Fig. 14. Jet 3 seems to be the most active in the cooling process by protecting the blade from the hot stream until a reduced absissa of 0.5 and then impacting the vane between 0.5 and 0.6.

The reduced temperature obtained during this work over-estimates experimental measurements. In particular, the strong acceleration caused by the blade induces large thermal gradients at the trailing edge. This phenomenon, not-well resolved by the computations, leads to a non-physical values of cooling efficiency. Nevertheless, these results have shown great sensitivity to multiple parameters, not only of the coupling strategy but also of the LES models for heat transfer and wall descriptions. Additional studies will be continued after the Summer Program.

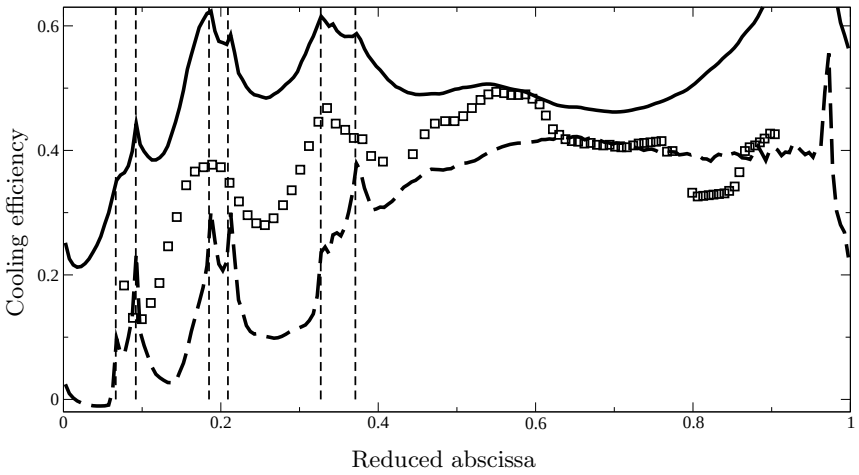

FIGURE 13. Cooling efficiency Θ versus abscissa on the pressure side at steady state. Dashed line: adiabatic LES, solid line: coupled LES, symbols: experiment from UNIBW, vertical dashed lines: position of the holes.

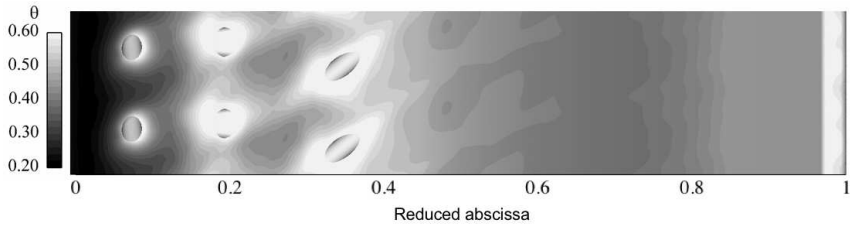

FIGURE 14. Spatial distribution of reduced temperature θ on the pressure side of the blade. The computational domain is duplicated one time in the z-direction.

5. Conclusions

Conjugate heat transfer calculations have been performed for two configurations of importance for the design of gas turbines with a recently developed massively parallel tool based on a LES solver. (1) An unsteady flame/wall interaction problem was used to assess the precision of coupled solutions when varying the coupling period. It was shown that the maximum coupling period that allows the temperature and the flux across the wall to reproduce well is of the order of the smallest time scale of the problem. (2) Steady convective heat transfer computation of an experimental film-cooled turbine vane showed how thermal conduction in the blade tends to reduce wall temperature compared to an adiabatic case. Further studies on LES models, coupling strategy and experimental conditions are needed to improve the quality of the results compared to the experimental cooling efficiency.

Acknowledgments

The help of L. Pons, from TURBOMECA, and of the AITEB-1 and AITEB-2 consortium regarding access to the experimental results is gratefully acknowledged.

REFERENCES

BOGARD, D. G. & THOLE, K. A. 2006 Gas turbine film cooling. *J. Prop. Power* **22** (2), 249–270.

BUIS, S., PIACENTINI, A. & DÉCLAT, D. 2005 PALM: A Computational Framework for assembling High Performance Computing Applications. *Concurrency and Computation: Practice and Experience* .

BUNKER, R. S. 2007 Gas turbine heat transfer: Ten remaining hot gas path challenges. *Journal of Turbomachinery* **129**, 193–201.

Chemin, S. 2006 Étude des interactions thermiques fluides-structure par un couplage de codes de calcul. PhD thesis, Université de Reims Champagne-Ardenne.

Colin, O. & Rudgyard, M. 2000 Development of high-order Taylor-Galerkin schemes for unsteady calculations. *J. Comput. Phys.* **162** (2), 338–371.

Dabireau, F., Cuenot, B., Vermorel, O. & Poinsot, T. 2003 Interaction of H2/O2 flames with inert walls. *Combust. Flame* **135** (1-2), 123–133.

Delataillade, A., Dabireau, F., Cuenot, B. & Poinsot, T. 2002 Flame/wall interaction and maximum heat wall fluxes in diffusion burners. *Proc. Combust. Inst.* **29**, 775–780.

Desoutter, G., Cuenot, B., Habchi, C. & Poinsot, T. 2005 Interaction of a premixed flame with a liquid fuel film on a wall. *Proc. Combust. Inst.* **30**, 259–267.

Ezekoye, O. A., Greif, R. & Lee, D. 1992 Increased surface temperature effects on wall heat transfer during unsteady flame quenching. In *24th Symp. (Int.) on Combustion*, pp. 1465–1472. The Combustion Institute, Pittsburgh, Penn.

Garg, V. 2002 Heat transfer research on gas turbine airfoils at NASA GRC. *International Journal of Heat and Fluid Flow* **23** (2), 109–136.

Giles, M. 1997 Stability analysis of numerical interface conditions in fluid-structure thermal analysis. *International Journal for Numerical Methods in Fluids* **25** (4), 421–436.

Holmer, M.-L., Eriksson, L.-E. & Sunden, B. 2000 Heat transfer on a film cooled inlet guide vane. In *Proceedings of the ASME Heat Transfer Division, American Society of Mechanical Engineers*, vol. 366-3, pp. 43–50. Orlando, Florida.

Lefebvre, A. H. 1999 *Gas Turbines Combustion*. Taylor & Francis.

Lu, J. H., Ezekoye, O., Greif, R. & Sawyer, F. 1990 Unsteady heat transfer during side wall quenching of a laminar flame. In *23rd Symp. (Int.) on Combustion*, pp. 441–446. The Combustion Institute, Pittsburgh, Penn.

Medic, G. & Durbin, P. A. 2002 Toward improved film cooling prediction. *J. Turbomach.* **124**, 193–199.

Mercier, E., Tesse, L. & Savary, N. 2006 3d full predictive thermal chain for gas turbine. In *25th International Congress of the Aeronautical Sciences*. Hamburg, Germany.

Moureau, V., Lartigue, G., Sommerer, Y., Angelberger, C., Colin, O. & Poinsot, T. 2005 High-order methods for DNS and LES of compressible multi-component reacting flows on fixed and moving grids. *J. Comput. Phys.* **202** (2), 710–736.

Nicoud, F. & Poinsot, T. 1999 DNS of a channel flow with variable properties. In *Int. Symp. On Turbulence and Shear Flow Phenomena.*. Santa Barbara, Calif.

Poinsot, T. & Veynante, D. 2005 *Theoretical and numerical combustion*. R.T. Edwards, 2nd edition.

Popp, P. & Baum, M. 1997 An analysis of wall heat fluxes, reaction mechanisms and unburnt hydrocarbons during the head-on quenching of a laminar methane flame. *Combust. Flame* **108** (3), 327–348.

Popp, P., Baum, M., Hilka, M. & Poinsot, T. 1996 A numerical study of laminar flame wall interaction with detailed chemistry: wall temperature effects. In *Rapport du Centre de Recherche sur la Combustion Turbulente* (ed. T. J. Poinsot, T. Baritaud & M. Baum), pp. 81–123. Rueil Malmaison: Technip.

Roux, A., Gicquel, L. Y. M., Sommerer, Y. & Poinsot, T. J. 2008 Large eddy simulation of mean and oscillating flow in a side-dump ramjet combustor. *Combust. Flame* **152** (1-2), 154–176.

Schiele, R. & Wittig, S. 2000 Gas turbine heat transfer: Past and future challenges. *Journal of Propulsion and Power* **16** (4), 583–589.

Schönfeld, T. & Rudgyard, M. 1999 Steady and unsteady flows simulations using the hybrid flow solver AVBP. *AIAA Journal* **37** (11), 1378–1385.